Monthly Notices of the ROYAL ASTRONOMICAL SOCIETY LETTERS

Mon. Not. R. Astron. Soc. **423,** L30–L34 (2012) doi:10.1111/j.1745-3933.2012.01251.x

A broad-band flux scale for low-frequency radio telescopes

Anna M. M. Scaife[1]★ and George H. Heald[2]

[1]*School of Physics & Astronomy, University of Southampton, Highfield, Southampton SO17 1BJ*
[2]*ASTRON, the Netherlands Institute for Radio Astronomy, Postbus 2, 7990 AA Dwingeloo, the Netherlands*

Accepted 2012 March 3. Received 2012 March 2; in original form 2012 February 27

ABSTRACT

We present parametrized broad-band spectral models valid at frequencies between 30 and 300 MHz for six bright radio sources selected from the 3C survey, spread in right ascension from 0 to 24 h. For each source, data from the literature are compiled and tied to a common flux density scale. These data are then used to parametrize an analytic polynomial spectral calibration model. The optimal polynomial order in each case is determined using the ratio of the Bayesian evidence for the candidate models. Maximum likelihood parameter values for each model are presented, with associated errors, and the percentage error in each model as a function of frequency is derived. These spectral models are intended as an initial reference for science from the new generation of low-frequency telescopes now coming online, with particular emphasis on the Low Frequency Array (LOFAR).

Key words: methods: observational – methods: statistical.

1 INTRODUCTION

In order to quantitatively combine and contrast data from independent telescopes and surveys, often at multiple frequencies, it is necessary to have a standard calibration scale to form comparisons. This is especially important at frequencies below 300 MHz and above 15 GHz where the widely used Baars et al. (1977) radio flux density scale is incomplete. For the new generation of low-frequency telescopes such as the Low Frequency Array (LOFAR; van Haarlem et al., in preparation), it is becoming increasingly necessary to provide a broad-band spectral reference for initial science, so that both archival and future measurements can be quantitatively compared to these new data. In addition to an absolute scaling, such telescopes require a well-defined set of calibrators spread in right ascension (RA) to allow for quasi-simultaneous broad-band calibration of field observations. Here we present a set of parametrized models for six broad-band calibrators covering frequencies from 30 to 300 MHz and RAs from 0 to 24 h. We focus on the northern sky, and in particular on the applicability to LOFAR. This set of calibrators forms a flux scale that will be the basis of a major effort to develop an all-sky, broad-band calibration catalogue. The initial description given here will be continuously refined as new LOFAR data accumulate.

2 CALIBRATION OF LOW-FREQUENCY TELESCOPES

Radio interferometers operating at low frequencies face a substantial calibration challenge. Strong ionospheric phase corruptions are common, especially below 100 MHz. For large-scale survey work in particular, it is important that the processing of raw visibility data from the telescope can be automated. In order to jump start such an automatic calibration and imaging process for any arbitrary field, a pre-existing model of the brightest sources in the field of view is required. Such a model must be intrinsically frequency-dependent, since modern radio telescopes are inherently broad band in nature, with tremendous fractional bandwidths. For example, LOFAR routinely observes from 30 to 240 MHz, and is capable of observing as low as 10 MHz. Over such a broad range, the flux scales must be tied to a well-understood set of reference sources with spectral energy distributions (SEDs) that are well understood across the full bandpass. In the case of LOFAR, the production of such an all-sky broad-band catalogue is the key goal of the Multifrequency Snapshot Sky Survey (MSSS; Heald et al., in preparation).

The reference sources which form the basis of the broad-band flux scale must be selected for suitability as high-quality calibration targets. Several factors are relevant. First, the source should dominate the visibility function. In addition to high flux density, separation of contaminating flux from sources away from the pointing centre ('off-beam') can be improved in two further ways: (i) averaging in time and frequency to smear out the contributions of off-beam sources on longer baselines and (ii) the 'demixing' technique (van der Tol, Jeffs & van der Veen 2007), which has been adopted for use with LOFAR data. Secondly, the source should be compact compared to the angular resolution of the instrument, to allow simple morphological calibration models. Well-known sources such as Cyg A and Cas A have extremely complex morphologies, making calibration of an array with arcsecond angular resolution difficult. Thirdly, these calibrators must be spread in RA to allow for quasi-simultaneous broad-band calibration with field observations.

With these considerations in mind we searched the 3C (Edge et al. 1959) and revised 3C (3CR; Bennet 1962) catalogues for an initial list of bright compact sources, with the criteria that (1) they must be

★E-mail: a.scaife@soton.ac.uk

Table 1. Calibration source sample.

Source	RA (J2000)	Dec. (J2000)	S_{3C} [a] (Jy)	$\Delta\theta$ [b] (arcsec)
3C 48	01 37 41.3	+33 09 35	50 ± 11	<1
3C 147	05 42 36.1	+49 51 07	63 ± 12	<12
3C 196	08 13 36.0	+48 13 03	66 ± 20	<12
3C 286	13 31 08.3	+30 30 33	21[b]	<3[c]
3C 295	14 11 20.5	+52 12 10	74 ± 15	<12
3C 380	18 29 31.8	+48 44 46	70 ± 10	<20

[a]Unadjusted flux densities at 159 MHz.
[b]Values from the 3CR catalogue (Bennet 1962).
[c] Pearson et al. (1985).

at declinations greater than 30°, (2) they must have a flux density at 178 MHz greater than 20 Jy and (3) they must have an angular diameter less than 20 arcsec (compact compared to the naturally weighted resolution of the Dutch LOFAR array).

These criteria result in an initial sample of six sources, of which we exclude one based on other data from the literature showing more substantial extension than indicated in 3CR (3C 69; Pooley & Henbest 1974) and we include one additional source based on other data from the literature indicating that the extension listed in 3CR is an overestimate (3C 286; e.g. Pearson, Readhead & Perley 1985). The final sample is listed in Table 1. Source extensions from 3CR are listed in column (5) for each object. We note that high-resolution observations (e.g. Akujor & Garrington 1995) confirm that the source structure in 3C 48 is on sub-arcsecond scales, whilst 3C 147, 3C 286 and 3C 295 have structure on scales <5 arcsec. 3C 196 has two dominant components separated by about 6 arcsec, as well as complex diffuse structure with a (precessing) jet morphology (Reid et al. 1995). The structure in 3C 380 is known to be dominant on scales of ≈16 arcsec, making it the most extended object in this sample (Reid et al. 1995).

3 FLUX SCALES

The data used for spectrum fitting are listed in Table 2. In order to provide a common flux scaling, these data have been revised on to the flux scale of Roger, Costain & Bridle (1973; hereafter RBC) below 325 MHz. This scale has been chosen to avoid the suggested issues (e.g. Rees 1990b) with the secular decrease in the flux density of Cas A at low frequencies (<100 MHz) inherent in the widely used Baars et al. (1977, hereafter B77) scale.

At low radio frequencies most data are tied to the RCB or Kellerman, Pauliny-Toth & Williams (1969, hereafter KPW) scales. The correction factors for moving between these scales at $\nu <$ 325 MHz are listed in Table. 2. At $\nu >$ 325 MHz the RCB and KPW scales are in agreement and consequently such data, when calibrated on the B77 scale, are corrected using a polynomial fit to the correction factors listed in B77 on to the KPW scale. Data from WENSS (Rengelink et al. 1997) have been corrected using an average correction factor to bring them on to the B77 scale and a further scaling to bring them on to the RCB scale. The 6C, 8C and MIYUN surveys are calibrated on the RCB scale in their original form, and the Bologna survey (Colla et al. 1970) is calibrated on the KPW scale which is consistent with the RCB at 408 MHz. Data from Aslanyan, Malumyan & Sanamyan (1968) are scaled using the ratio of the stated flux densities for the calibrator sources (3C 348 and 3C 353) in the original paper to the predicted values at 60 MHz from the spectral models for these sources in RCB. Data from Scott & Shakeshaft (1971) are corrected on to the scale of Artyukh et al. (1969) and then on to the RCB scale using the factors listed in tables III and IV of RCB; this is subject to the caveat that the difference in flux densities from 81.5 to 86 MHz is assumed to be negligible compared to the uncertainty in these factors (≈3 per cent). Where applied, the scaling factors in each case are listed in Table 2. The original flux densities for the sources from the 3C catalogue (Edge et al. 1959) have not been included in the model fitting. The large size of the errors associated with these data is such that they have no influence on the parameter estimation.

Table 2. References for data used in spectral fitting. Columns are follows: (1) frequency; (2) reference; (3) correction factor applied to original data for conversion to RCB flux scale.

Freq. (MHz)	Ref.	Factor
10	Bridle & Purton (1968)	1.20[a]
	RCB	–
22.25	Roger, Costain & Lacey (1969)	1.15[a]
	RCB	–
38	KPW	1.18[a]
	Rees (1990a) (8C)	–
60	Aslanyan et al. (1968)	1.04[b]
81.5	Scott & Shakeshaft (1971)	0.90[b]
86	Artyukh et al. (1969)	0.94[a]
151	Baldwin et al. (1985) (6C)	–
178	KPW	1.09[a]
232	Zhang et al. (1997) (MIYUN)	–
325	Rengelink et al. (1997) (WENSS)	0.90[b]
408	Colla et al. (1970)	–
750	KPW	–
960	Kovalev (1997)	0.96[c]
1400	KPW	–

[a]From RCB;
[b]see text for details;
[c]from B77.

Additional data are available at 12.6–25 MHz from the UTR-1 telescope (Braude et al. 1970a,b), calibrated on the Gravoko scale. These data have not been used in the fitting, primarily because the discrepancy between the Gravoko and RCB flux scales is not only frequency-dependent but also flux density-dependent and there is no complete revision scale available. For a discussion see RCB.

4 SPECTRAL MODEL

A spectral model of the form

$$\log S = \log A_0 + A_1 \log \nu + A_2 \log^2 \nu + \cdots$$

was used. The model was applied in linear frequency space, i.e.

$$S[\mathrm{Jy}] = A_0 \prod_{i=1}^{N} 10^{A_i \log^i [\nu/150\,\mathrm{MHz}]},$$

in order to retain Gaussian noise characteristics. Both determination of the optimal order (N) of polynomial model and maximum likelihood (ML) parameter estimation were performed using a Markov chain Monte Carlo implementation. We used a simulated annealing method, through the METRO algorithm (Hobson & Baldwin 2004) to employ a Bayesian inference approach, where Bayes formula,

$$\Pr(\Theta|D, H) \equiv \frac{\Pr(D|\Theta, H)\Pr(\Theta|H)}{\Pr(D|H)},$$

is used to test a hypothesis, H, parametrized by Θ using a set of data, D. Here $\Pr(\Theta|D, H) \equiv P(\Theta)$ is the posterior probability distribution of the parameters, $\Pr(D|\Theta, H) \equiv \mathcal{L}(\Theta)$ is the likelihood and $\Pr(\Theta|H) \equiv \Pi(\Theta)$ is the prior probability distribution, which in this case is simply used to restrict the volume of parameter space being sampled.

The Bayesian evidence, $\Pr(D|H) \equiv Z$, is a factor required for normalizing the posterior over the prior volume, such that

$$Z = \int \mathcal{L}(\Theta)\Pi(\Theta)\mathrm{d}^M\Theta,$$

where M is the dimensionality of the prior volume; here $M = N + 1$. For parameter estimation the evidence factor can be neglected as it is independent of the model parameters. ML or maximum a posteriori (MAP) parameter values can be obtained by sampling the normalized distribution in each case to determine the peak in parameter space. However, in model selection the evidence becomes important for ranking different models based on a common data set. It can be seen from the previous equation that the evidence represents the average of the likelihood over the prior, and therefore favours models with high likelihood values throughout the parameter space and penalizes models with regions of very low likelihood. This is equivalent to numerically implementing Occam's razor, whereby larger evidence values are returned for simple models (i.e. fewer parameters) with compact parameter spaces, compared to more complex models – unless the more complex model provides a significantly better fit to the data.

Selecting between models, say H_0 and H_1, based on their evidence can be done using the ratio

$$\frac{\Pr(H_0|D)}{\Pr(H_1|D)} = \frac{\Pr(D|H_0)\Pr(H_0)}{\Pr(D|H_1)\Pr(H_1)} = \frac{Z_0}{Z_1}\frac{\Pr(H_0)}{\Pr(H_1)},$$

where $\Pr(H_0)/\Pr(H_1)$ is the ratio of prior probabilities. This ratio can be set before any conclusions have been drawn from the data; in many cases there is no reason to favour one particular model a priori and consequently this factor can be set to unity. In this circumstance the model selection can be based solely on the ratio of evidences.

In this work, for each model, priors were assumed to be uniform and separable, and ML (MAP) parameters were determined initially using the METRO sampling algorithm. Once parameter values had been determined, the evidence in each case, Z, was calculated over a $\pm 3\sigma$ prior volume centred on the ML parameter values, with σ determined for each parameter directly from the posterior distribution. The evidence calculation was repeated multiple times in each case in order to assess the variance of the evidence. Evidence ratios (also known as Bayes factors, or the odds) were then used to determine the optimal polynomial fit based on the Jeffreys scale (Jeffreys 1961); see Section 4.1. In practice, we take $\Delta\ln Z > 1$ as our threshold for selecting the best model; this choice is justified in Section 5.

4.1 Requirements for model selection

The requirement to use a model of increased complexity (i.e. polynomial of higher order) depends upon the degree to which the evidence increases relative to the next lowest order; see column (9) of Table 3. On the original Jeffreys scale (Jeffreys 1961) an increase of a factor of 3 (i.e. $\Delta\ln Z \geq 3$) is considered substantial evidence

Table 3. Column (1) lists the order of the polynomial fit; columns (2)–(6) list the fitted ML polynomial coefficients; column (7) lists the reduced χ^2 value; column (8) lists the natural logarithm of the evidence for a 3σ prior volume. The selected best-fitting model is highlighted in each case.

Order	A_0	A_1	A_2	A_3	A_4	$\chi^2_{\rm red}$	$\ln Z$	$\Delta(\ln Z)$
3C 48								
1°	43.874 ± 0.879	-0.349 ± 0.011	–	–	–	21.68	-135.00 ± 0.03	–
2°	62.821 ± 1.642	-0.284 ± 0.015	-0.374 ± 0.026	–	–	1.16	-33.02 ± 0.06	101.98
3°	64.768 ± 1.761	-0.387 ± 0.039	-0.420 ± 0.031	0.181 ± 0.060	–	0.10	-29.86 ± 0.23	3.16
4°	63.910 ± 1.864	-0.394 ± 0.045	-0.391 ± 0.093	0.185 ± 0.075	-0.014 ± 0.118	0.15	-33.41 ± 0.47	-3.55
3C 147								
2°	60.517 ± 1.474	0.016 ± 0.028	-0.514 ± 0.046	–	–	2.35	-35.28 ± 0.14	–
3°	66.738 ± 2.490	-0.022 ± 0.030	-1.012 ± 0.167	0.549 ± 0.170	–	0.24	-29.59 ± 0.47	5.69
4°	66.494 ± 1.915	-0.041 ± 0.046	-0.952 ± 0.109	0.625 ± 0.245	-0.124 ± 0.249	0.26	-30.15 ± 0.48	-0.59
3C 196								
1°	76.641 ± 1.227	-0.719 ± 0.012	–	–	–	2.80	-47.25 ± 0.08	–
2°	83.084 ± 1.862	-0.699 ± 0.014	-0.110 ± 0.024	–	–	0.51	-36.89 ± 0.09	10.36
3°	83.011 ± 1.787	-0.676 ± 0.029	-0.107 ± 0.023	-0.039 ± 0.041	–	0.50	-38.16 ± 0.14	-1.27
4°	83.776 ± 2.214	-0.677 ± 0.033	-0.139 ± 0.073	-0.027 ± 0.045	0.035 ± 0.073	0.54	-40.37 ± 0.50	-2.21
3C 286								
1°	27.893 ± 0.653	-0.258 ± 0.017	–	–	–	1.46	-33.93 ± 0.08	–
2°	28.230 ± 0.708	-0.208 ± 0.035	-0.077 ± 0.045	–	–	1.32	-34.09 ± 0.14	-0.16
3°	27.477 ± 0.746	-0.158 ± 0.033	0.032 ± 0.043	-0.180 ± 0.052	–	0.42	-30.51 ± 0.21	3.58
4°	27.591 ± 0.911	-0.144 ± 0.038	0.005 ± 0.097	-0.187 ± 0.054	0.021 ± 0.086	0.48	-32.58 ± 0.49	-2.07
3C 295								
2°	97.489 ± 2.177	-0.347 ± 0.016	-0.362 ± 0.028	–	–	6.12	-49.27 ± 0.07	–
3°	100.950 ± 2.454	-0.517 ± 0.035	-0.497 ± 0.041	0.360 ± 0.066	–	1.85	-35.46 ± 0.26	13.81
4°	97.763 ± 2.787	-0.582 ± 0.045	-0.298 ± 0.085	0.583 ± 0.116	-0.363 ± 0.137	1.00	-33.86 ± 0.34	1.60
5°	–	–	–	–	–	1.30	-36.33 ± 0.22	-2.47
3C 380								
1°	77.352 ± 1.164	-0.767 ± 0.013	–	–	–	1.20	-38.11 ± 0.06	–
2°	75.682 ± 1.537	-0.772 ± 0.012	0.039 ± 0.021	–	–	1.02	-37.47 ± 0.10	0.64
3°	75.233 ± 1.483	-0.788 ± 0.033	0.041 ± 0.020	0.024 ± 0.047	–	1.11	-39.22 ± 0.15	-1.75
4°	74.386 ± 1.595	-0.787 ± 0.034	0.104 ± 0.067	0.030 ± 0.051	-0.084 ± 0.082	1.14	-40.96 ± 0.40	-1.74

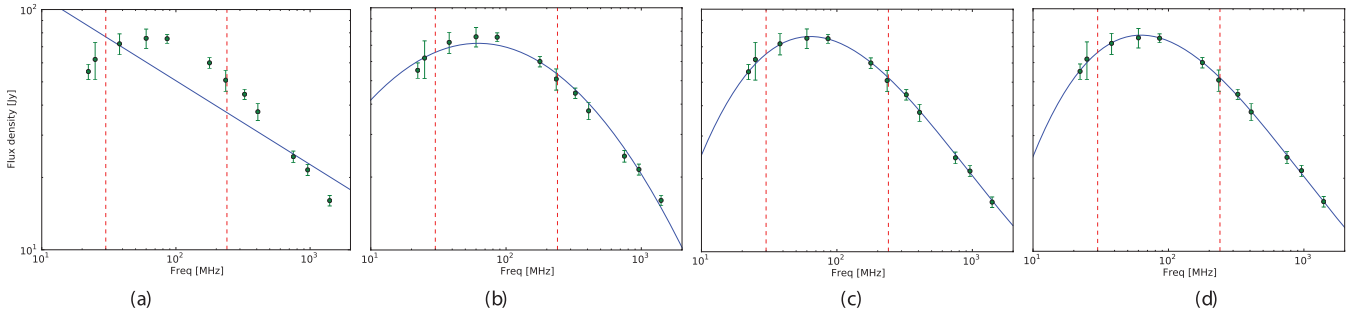

Figure 1. 3C48 SED. (a) Data fitted with linear (1°) model, (b) data fitted with second-order model, (c) data fitted with third-order model and (d) data fitted with fourth-order model. ML parameters for each fit are listed in Table 3. Dashed lines indicate the upper and lower bounds of the LOFAR frequency band.

to prefer the higher order model and can be considered equivalent to a 99.7 per cent confidence result. Revised versions of the Jeffreys scale (e.g. Gordon & Trotta 2007) divide the level of support into categories where it is considered as either 'inconclusive' ($\Delta \ln Z < 1$), 'weak' ($1 \leq \Delta \ln Z \leq 2.5$), 'moderate' ($2.5 \leq \Delta \ln Z \leq 5$) or 'strong' ($\Delta \ln Z \geq 5$).

5 RESULTS

The ML parameters and evidence values for each polynomial fit to the source spectra are listed in Table 3. An example of the different orders is shown for 3C 48 in Fig. 1. The poor fit of the linear and 2° polynomial model is evident by eye. This is also reflected in the values of the evidence for these models: an evidence ratio, and hence difference in the logarithm of the evidence, of $\ln Z_{3^\circ} - \ln Z_{1^\circ} > 100$ indicates a definitive preference; a difference of $\ln Z_{3^\circ} - \ln Z_{2^\circ} = 3.16$ is substantial evidence for preferring the 3° model above the 2° model. The fractional evidence ratio, $\ln Z_{4^\circ} - \ln Z_{3^\circ} = -3.55$, between the 4° and 3° polynomial models indicates that the 3° model is still preferred. In this case the goodness of fit is not diminished by the 4° model, but there is no evidence in the data to support the use of the extra parameter and hence the model is penalized.

In general, the results for this sample are easily interpreted, with Bayes factors of $\Delta \ln Z > 3$ clearly indicating a preferred order of polynomial in most cases. When comparing different polynomial order fits to the 3C 295 and 3C 380 data sets, the Bayes factors are less conclusive than in other cases. A difference of $\Delta \ln Z = 1.6$ between the third- and fourth-order models in the case of 3C 295 is intermediate to the 'weak support' category. Although the support for moving to the higher order model is weak, it is not inconclusive and so in the context of the work here we choose to prefer the fourth-order model. In the case of 3C 380, a value of $\Delta \ln Z = 0.64$ is securely in the inconclusive category and so we prefer the lower order model in this instance. Best-fitting spectral models for the six calibrator sources are shown in Fig. 2.

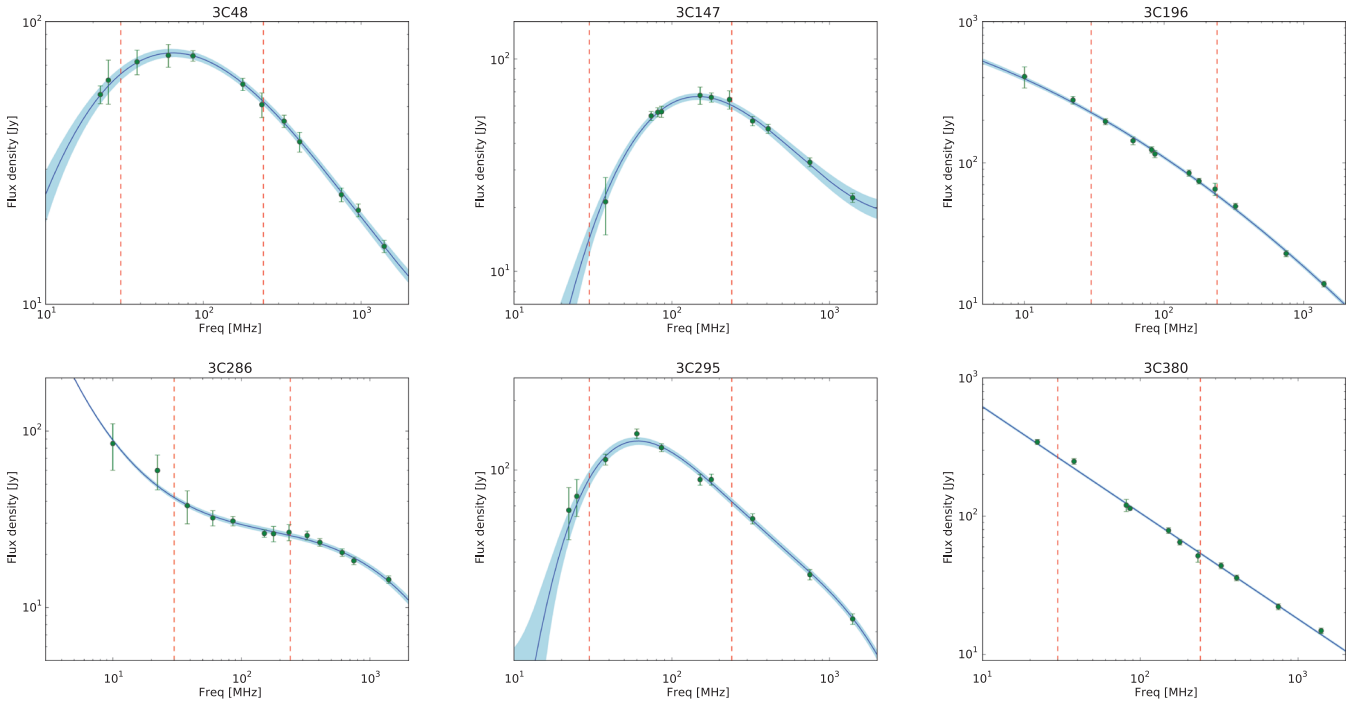

Figure 2. Best-fitting models for calibrator sources. Data from the literature are shown in black with the selected best-fitting model overlaid as a solid line. The area enclosed by the shaded region indicates the flux densities allowed at each frequency by 1σ uncertainties on the parameters. The edges of the LOFAR bandpass (low and high bands) are indicated by vertical dashed lines.

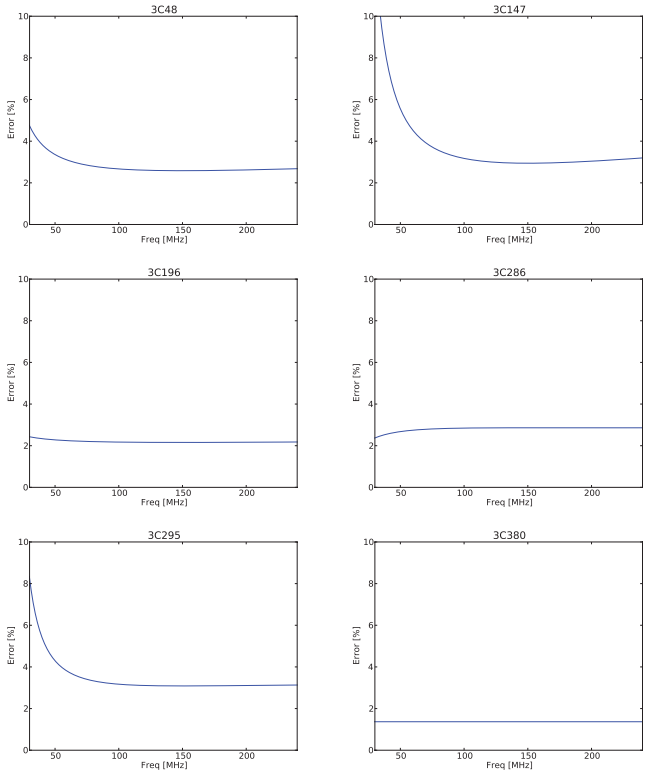

Figure 3. Percentage error in each model as a function of frequency from 30 to 240 MHz.

5.1 Error budget

Errors on individual parameters for each fit were determined directly from the posterior distribution and are listed in Table 3. The uncertainty in the model due to these errors was derived analytically using differential error propagation, and the 1σ bound on the model in each case is illustrated in Fig. 2 as a blue shaded area. We illustrate the percentage error of each model as a function of frequency from 30 to 240 MHz (the LOFAR band) in Fig. 3. It can be seen that from currently available data not all of the six calibrators are suitable for calibration at the low end of this frequency range (e.g. 3C 147 and 3C 295), where their models possess high percentage uncertainty.

5.2 Notes on individual sources

The source 3C 380 has data at 10 MHz in Bridle & Purton (1968), but the very low flux density (168 Jy) indicates that the spectrum turns over sharply below 20 MHz. The effect of this turnover is marginal above 30, but would require significantly increased complexity in the model. Consequently, these data have been excluded from the fit.

6 CONCLUSIONS

We have presented parametrized broad-band spectral models for six bright radio sources selected from the 3C survey between 30 and 300 MHz, spread in RA from 0 to 24 h. For each source, data from the literature have been compiled and tied to a common flux density scale. These data have then been used to parametrize an analytic polynomial spectral calibration model. The best-fitting polynomial model order in each case has been determined using the ratio of the Bayesian evidence for the candidate models. ML parameter values with associated errors have been presented. The percentage error in each model as a function of frequency has been derived and is illustrated in Section 5.1. These spectral models are intended as an initial reference for science quality data from the new generation of low-frequency telescopes, such as LOFAR, now coming online. In this context we have shown that two of these sources lead to unacceptably high flux scale uncertainty at frequencies below 70 MHz (3C 147 and 3C 295), and we also note that 3C 380 may be unsuitable for precision calibration at higher frequencies where its angular extent becomes an issue.

ACKNOWLEDGMENTS

We thank Julia Riley and Ger de Bruyn for useful discussions and Rick Perley for his careful review of the manuscript. This research has made use of the Astrophysical CATalogs Support System (CATS; Verkhodanov et al. 2005) and the NASA/IPAC Extragalactic Database (NED), which is operated by JPL, under contract with NASA.

REFERENCES

Akujor C. E., Garrington S. T., 1995, A&AS, 112, 235
Artyukh V. S., Dagkesamanskii V. V., Vitkevich R. D., Kozhukhov V. N., 1969, SvA, 12, 567
Aslanyan A. M., Malumyan V. G., Sanamyan V. A., 1968, ApJ, 4, 252
Baars J. W. M., Genzel R., Pauliny-Toth I. I. K., Witzel A., 1977, A&A, 61, 99 (B77)
Baldwin J. E., Boysen R. C., Hales S. E. G., Jennings J. E., Waggett P. C., Warner P. J., Wilson D. M. A., 1985, MNRAS, 217, 717
Bennet A. S., 1962, Mem. R. Astron. Soc., 68, 163
Braude S. Y., Lebedeva O. M., Megn A. V., Ryabov B. P., Zhouck I. N., 1970a, ApJ, 5, L129
Braude S. Y., Megn A. V., Ryabov B. P., Zhouck I. N., 1970b, Ap&SS, 8, 275
Bridle A. H., Purton C. R., 1968, AJ, 73, 717
Colla G. et al., 1970, A&AS, 1, 281
Edge D. O., Shakeshaft J. R., McAdam W. B., Baldwin J. E., Archer S., 1959, Mem. R. Astron. Soc., 68, 37
Gordon C., Trotta R., 2007, MNRAS, 382, 1859
Hobson M. P., Baldwin J. E., 2004, Applied Opt., 43, 2651
Jeffreys H., 1961, Theory of Probability, 3rd edn. Clarendon Press, Oxford
Kellerman K. I., Pauliny-Toth I. I. K., Williams P. J. S., 1969, ApJ, 157, 1 (KPW)
Kovalev Y. A., 1997, Bull. Special Astrophys. Obser., 44, 50
Pearson T. J., Readhead A. C. S., Perley R. A., 1985, AJ, 90, 738
Pooley G. G., Henbest S. N., 1974, MNRAS, 169, 477
Rees N., 1990a, MNRAS, 243, 637
Rees N., 1990b, MNRAS, 244, 233
Reid A., Shone D. L., Akujor C. E., Browne I. W. A., Murphy D. W., Pedelty J., Rudnick L., Walsh D., 1995, A&AS, 110, 213
Rengelink R. B., Tang Y., de Bruyn A. G., Miley G. K., Bremer M. N., Roettgering H. J. A., Bremer M. A. R., 1997, A&AS, 124, 259
Roger R. S., Costain C. H., Lacey J. D., 1969, AJ, 74, 366
Roger R. S., Costain C. H., Bridle A. H., 1973, AJ, 78, 1030 (RCB)
Scott P. F., Shakeshaft J. R., 1971, MNRAS, 154, 19P
van der Tol S., Jeffs B. D., van der Veen A.-J., 2007, IEEE Trans. Signal Processing, 55, 4497
Verkhodanov O. V., Trushkin S. A., Andernach H., Chernenkov V. N., 2005, Bulletin SAO, No 58, 118–129 (arXiv:0705.2959)
Zhang X., Zheng Y., Chen H., Wang S., Cao A., Peng B., Nan R., 1997, A&AS, 121, 59

This paper has been typeset from a TEX/LATEX file prepared by the author.